Analytical Cellular Pathology 36 (2013) 45–59
DOI 10.3233/ACP-130078
IOS Press

The impact of the condenser on cytogenetic image quality in digital microscope system

Liqiang Ren[a], Zheng Li[a], Yuhua Li[a], Bin Zheng[b], Shibo Li[c], Xiaodong Chen[d] and Hong Liu[a,*]

[a]*Center for Bioengineering and School of Electrical and Computer Engineering, University of Oklahoma, Norman, OK, USA*

[b]*Deptartment of Radiology, University of Pittsburgh, Pittsburgh, PA, USA*

[c]*Department of Pediatrics and Department of Pathology, University of Oklahoma Health Sciences Center, Oklahoma City, OK, USA*

[d]*College of Precision Instruments and Opto-electronics Engineering, Tianjin University, Tianjin, China*

Abstract.

BACKGROUND: Optimizing operational parameters of the digital microscope system is an important technique to acquire high quality cytogenetic images and facilitate the process of karyotyping so that the efficiency and accuracy of diagnosis can be improved.

OBJECTIVE: This study investigated the impact of the condenser on cytogenetic image quality and system working performance using a prototype digital microscope image scanning system.

METHODS: Both theoretical analysis and experimental validations through objectively evaluating a resolution test chart and subjectively observing large numbers of specimen were conducted.

RESULTS: The results show that the optimal image quality and large depth of field (DOF) are simultaneously obtained when the numerical aperture of condenser is set as 60%–70% of the corresponding objective. Under this condition, more analyzable chromosomes and diagnostic information are obtained. As a result, the system shows higher working stability and less restriction for the implementation of algorithms such as autofocusing especially when the system is designed to achieve high throughput continuous image scanning.

CONCLUSIONS: Although the above quantitative results were obtained using a specific prototype system under the experimental conditions reported in this paper, the presented evaluation methodologies can provide valuable guidelines for optimizing operational parameters in cytogenetic imaging using the high throughput continuous scanning microscopes in clinical practice.

Keywords: Optimizing operational parameters, microscope condenser, image sharpness, resolution, depth of field (DOF), cytogenetic imaging

1. Introduction

Karyotyping of human chromosomes based on microscopic cytogenetic imaging has been routinely performed in cytogenetic laboratories as a standard procedure in diagnosis of cancers and genetic disorders through the analysis of chromosome pattern changes and/or aberration [1–3]. Therefore, acquiring cytogenetic images with sufficient band pattern sharpness and high resolution is important and helpful to improve disease diagnosis accuracy and efficiency in analyzing automatically scanned and acquired digital microscopic images [4]. For this purpose, much research efforts have been made focusing on developing high throughput microscopic image scanning

*Corresponding author: Hong Liu, Center for Bioengineering and School of Electrical and Computer Engineering, University of Oklahoma, 101 David L Boren Blvd, Norman, OK 73019, USA. Tel.: +1 405 325 4286; Fax: +1 405 325 7066; E-mail: liu@ou.edu.

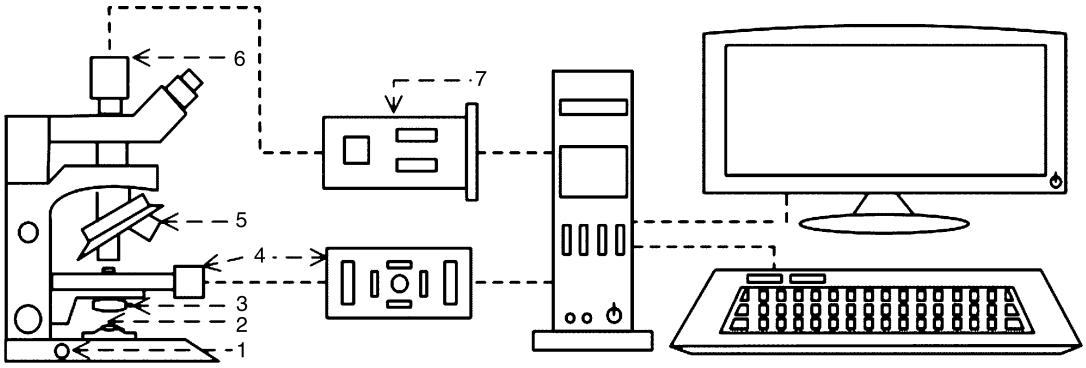

Fig. 1. Schematics of the prototype system configuration: 1-illumination intensity adjustment; 2-position for light intensity measurement; 3-condenser and its aperture diaphragm; 4-motorized microscope stage; 5-objectives; 6-CCD; 7-frame grabber.

systems and the computer aided detection (CAD) schemes to assist selection of analyzable metaphase chromosomes and conduct related image process tasks in recent years [5–7]. Among these efforts, optimizing operational parameters becomes a critical issue to achieve the accurate and reliable process of high throughput and continuous image scanning, which will also help improve the efficiency of chromosome identification and classification. Although the quality of scanned high-resolution microscopic images can be affected by optimally design of many optical and mechanical components, the microscope condenser is an important component. However, its impact on cytogenetic imaging quality and more importantly on the working stability of the high throughput microscope has not been fully investigated in this clinical application field.

In optical microscopes, the principal functions of the condenser are not only to provide even illumination over the entire field of view (FOV), but also to control the intensity and the angle of light entering the objective front lens. Therefore, appropriate aperture adjustment of the condenser is of critical significance in realizing the potential of the corresponding objective and even the whole digital microscope system [8]. Although several conclusions regarding the impacts of the condenser used in the conventional microscopes have been derived over the past years, these were only based on pure theoretical analysis or operational experiences that didn't provide a complete understanding over the impact of the condenser used in a dynamically image scanning microscopic system [8–16]. In this study, we systematically investigated the relationship between the condenser and the corresponding objective lens used in a high throughout microscopic image scanning system. Both theoretical analysis and experimental validations were conducted using a specific microscopic image scanning prototype system previously developed in our laboratory to evaluate the impacts of the condenser parameter variation on the image quality and then determine the optimal parameter of the condenser. The detailed analysis methods and experimental results are presented in the following sections of this article.

2. Materials and methods

2.1. Prototype system configuration

As shown in Fig. 1, the prototype microscopic imaging system is built based on an ordinary transmitted optical bright-field microscope (Eclipse, 50i, NIKON, Tokyo, JPN) with added high-resolution CCD (CM-141MCL, JAI, Yokohama, JPN), frame grabber (X64-CL, DALSA, Waterloo, CA) and motorized microscope stage (Prior, OptiScan II, Cambridge, UK).

In this prototype system, the illumination intensity from the light source can be adjusted through rotating part 1 and measured in position 2. A specific instrument, Light-O-Meter (CE0413, UNFORS INSTRUMENTS, Billdal, Sweden) for measuring luminance (cd/m^2) is used to provide qualitative reference. The NA_{cond} of the condenser (part 3, Abbe, dry) is up to 0.90. This is the reason why the two objectives used in this investigation are dry and both of their numerical apertures are below 0.90: 10× (dry, $NA_{obj} = 0.25$), 40× (dry, $NA_{obj} = 0.75$) [8, 17].

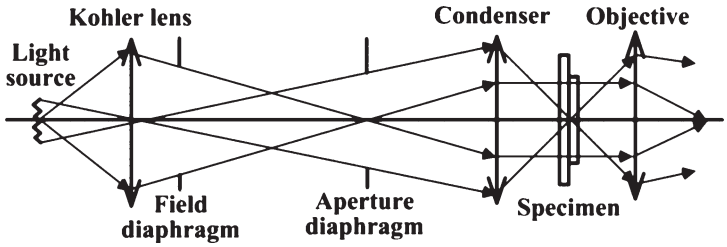

Fig. 2. The schematic relation between the Abbe condenser and the objective in the Kohler illumination.

2.2. Condenser impact on image sharpness and the measuring method

The default Abbe condenser equipped in this prototype system is mainly used for routine observation and is the simplest and least corrected one compared with Aplanatic, Achromatic and Aplanatic-Achromatic condensers [17]. The schematic relationship between the Abbe condenser and the objective in the Kohler illumination system is illustrated in Fig. 2 [18]. In this figure, light from the illumination source is concentrated and controlled by the aperture diaphragm of the condenser prior to passing through the specimen and entering the objective. Through adjusting the aperture diaphragm, an inverted light cone with proper size and angle is available to fill the objective [8]. If the aperture diaphragm is opened too wide regarding to that of the objective, flare (stray light) due to the internal reflection from oblique rays in the specimen reduces the image sharpness [19]. On the other hand, if the aperture diaphragm is closed too far, the illumination intensity is insufficient and there is a danger of introducing optical artifacts [20]. An optimal size of aperture diaphragm of the condenser, therefore, is very important to obtain the best image sharpness.

The 1951 USAF resolution test chart (Edmund Optics, New jersey, US) consisting of gradual change of spatial frequency from 1.00 lp/mm to 645.0 lp/mm was used to objectively evaluate the condenser impact on image sharpness under 10× and 40× objectives, respectively. During the image sharpness evaluations, three various spatial frequency groups from 3.56 lp/mm to 645.0 lp/mm and a proper range of illumination intensity L = 2000–5000 cd/m^2 were applied for evaluating the 10× objective, while the spatial frequencies ranged from 16.00 lp/mm to 645.0 lp/mm and the illumination intensity L = 7000–10000 cd/m^2 for the 40× objective.

An evaluation function in spatial domain is adopted to measure the image sharpness. The calculating formula is shown as below [21]:

$$S = \frac{1}{4(m-2)(n-2)} \sum_{i=2}^{m-1} \sum_{j=2}^{n-1} \left\{ \begin{array}{l} [f(i+1,\ j) - f(i,\ j)]^2 + [f(i,\ j+1) - f(i,\ j)]^2 \\ + [f(i,\ j) - f(i-1,\ j)]^2 + [f(i,\ j) - f(i,\ j-1)]^2 \end{array} \right\} \quad (1)$$

Where S represents the image sharpness; $f(i,\ j)$ is the gray value at pixel $(i,\ j)$; m and n are the numbers of rows and columns of image f. The calculating process of equation (1) is based on 4 adjoining points and the final result S is obtained as an average value by dividing $4(m-2)(n-2)$, which is the total number of subtraction operations.

2.3. Condenser impact on resolution and the measuring method

The resolution of the microscope, which is typically represented by the smallest distance between two adjacent and distinguishable points, is an important influencing factor of chromosome analysis [4, 22]. According to Rayleigh criteria, the most widely accepted formula for calculating the resolution of microscopes under incoherent illumination is:

$$\delta = \frac{0.61\lambda}{NA_{obj}} \quad (2)$$

where δ is the resolution, λ is the wavelength of the light used in the microscope and is assumed to be 0.55 μm here, and NA_{obj} is the numerical aperture of the objective.

Although Equation (2) gives the basic resolution equation of the microscope, it is only valid under the condition of $NA_{cond} \geq NA_{obj}$ when considering the impact of the condenser on resolution. An effective

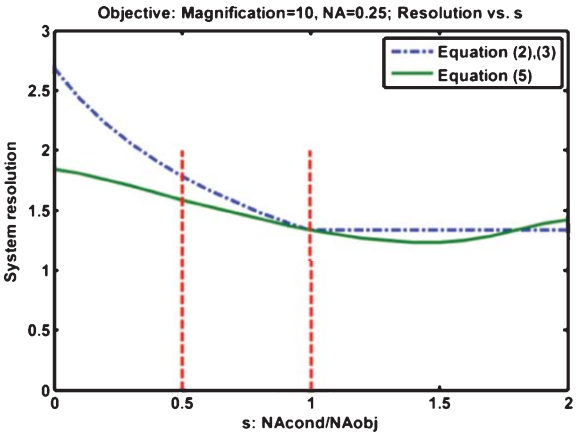

Fig. 3. Thetheoretical relation between resolution and s under 10× ($NA_{obj} = 0.25$) based on Equations (2), (3) and (5); two red lines show that in the range of $s = 0.5$–1.0, the result from Equations (2) and (3) is approximately close to that from Equation (5).

NA can be computed as the mean of the NA_{cond} and NA_{obj} in the case where $NA_{cond} \leq NA_{obj}$. Therefore, Equation (3) is the version of the resolution formula when $NA_{cond} \leq NA_{obj}$ [10–12]:

$$\delta = \frac{1.22\lambda}{NA_{obj} + NA_{cond}} \tag{3}$$

Where NA_{cond} and NA_{obj} are the numerical apertures of the objective and the condenser, respectively. According to Equations (2) and (3), the best resolution in theory obtained when $NA_{cond} \geq NA_{obj}$ is shown in Fig. 3, in which s denotes the NA_{cond} of the condenser dividing by NA_{obj} of the corresponding objective.

Based on the condition of partially coherent illumination, an alternative opinion is derived by Hopkins and Barham [13, 23]. In their theory, two pinholes $P_1(X_1, Y_1)$ and $P_2(X_2, Y_2)$ in the plane of the object are considered to estimate the effect of the size of the condenser on the resolution. The complex degree of coherence of the light that reaches the two pinholes from the light source is given as:

$$j(P_1,\ P_2) = \frac{2J_1(u_{12})}{u_{12}},$$
$$u_{12} = \frac{2\pi NA_{cond}}{\lambda}\sqrt{(X_1 - X_2)^2 + (Y_1 - Y_2)^2} \tag{4}$$

Let $P(X,\ Y)$ be any other point in the object plane, and P' be its image by the objective. Thus, the intensity $I(P')$ in the image plane of the microscope objective is equal to the sum of the intensity $I^{(1)}(P')$ reaching from P_1 alone, the intensity $I^{(2)}(P')$ reaching from P_2 alone and the intensity $I^{(12)}(P')$ due to the partially coherence of the two beams:

$$\begin{aligned} I(P') &= I^{(1)}(P') + I^{(2)}(P') + I^{(12)}(P') \\ &= \left[\frac{2J_1(v_1)}{v_1}\right]^2 + \left[\frac{2J_1(v_2)}{v_2}\right]^2 \\ &\quad + 2\left[\frac{2J_1(sv_{12})}{sv_{12}}\right]\left[\frac{2J_1(v_1)}{v_1}\right]\left[\frac{2J_1(v_2)}{v_2}\right] \end{aligned} \tag{5}$$

Where

$$v_1 = \frac{2\pi NA_{obj}}{\lambda}\sqrt{(X - X_1)^2 + (Y - Y_1)^2} \tag{6}$$

$$v_2 = \frac{2\pi NA_{obj}}{\lambda}\sqrt{(X - X_2)^2 + (Y - Y_2)^2} \tag{7}$$

$$v_{12} = \frac{u_{12}}{s} = \frac{2\pi NA_{obj}}{\lambda}\sqrt{(X_1 - X_2)^2 + (Y_1 - Y_2)^2} \tag{8}$$

$$s = \frac{NA_{cond}}{NA_{obj}} \tag{9}$$

When NA_{cond} is very small ($s \to 0$), then $2J_1(sv_{12})/sv_{12} \approx 1$ and Equation (5) therefore reduces to Equation (10) and now the distribution of the intensity is the same as with perfectly coherent illumination.

$$I(P') = \left[\frac{2J_1(v_1)}{v_1} + \frac{2J_1(v_2)}{v_2}\right]^2 \tag{10}$$

If it is the case when $s = 1$ and v_{12} is a nonzero root of $J_1(sv_{12}) = 0$, the distribution of the intensity in the image plane is now the same as if $P_1(X_1, Y_1)$ and $P_2(X_2,\ Y_2)$ are illuminated incoherently. Thus, the product term is absent and Equation (5) reduces to

$$\begin{aligned} I(P') &= I^{(1)}(P') + I^{(2)}(P') \\ &= \left[\frac{2J_1(v_1)}{v_1}\right]^2 + \left[\frac{2J_1(v_2)}{v_2}\right]^2 \end{aligned} \tag{11}$$

Based on the preceding discussion, the illumination condition changes from perfectly coherent light when $s = 0$ to completely incoherent light when $s = 1$ and is partially coherent in the range from $s = 0$ to $s = 1$. Also, the illumination light should still be seen as incoherent light when $s > 1$ because it has been completely incoherent when s is equal to 1. Although it is possible to

study the dependence of the intensity distribution at the midpoint between P_1' and P_2' in the image plane of the microscope objective on the ratio s and to plot the relation curve in Fig. 3 using Equation (5) from the mathematical viewpoint, it is hard to convince people of the physical meaning that the system can reach higher resolution, because the illumination condition can't change back to be partially coherent or completely coherent again and the product term in Equation (5) can't become a negative term under inherent illumination when $s > 1$. Therefore, only the conclusion when s is between 0 and 1 can be applied to evaluate the system resolution of a practical microscope system. In Fig. 3, it is also shown from the two viewpoints that the results obtained from Equations (2) and (3) can give a rough approximation especially when s is set in the range from 0.5 to 1.

When the theories are applied to evaluate practical systems, however, it should be noticed that any points on the object can't be treated as ideal pinholes. Flare (stray light) due to the sample non-uniformity and the internal reflection from oblique rays in the specimen would disturb the imaging process especially under the condition that $NA_{cond} \geq NA_{obj}$ ($s \geq 1$). Actually, the flare (stray light) would lower the contrast and then reduce the resolving power if the aperture of the condenser is opened larger than that of the objective. The theoretical hypothesis here is that the optimal size or range of the condenser aperture should be a little smaller than that when $s = 1$, in an effort to reduce the flare light while providing sufficient illumination intensity. The optimal size or range of the condenser aperture for the best resolution needs to be verified by comprehensive experiments under different s value and illumination intensity.

The 1951 USAF resolution test chart was then applied to measure the contrast transfer function (CTF) under the condition of using a 10× objective, different s value from 0.2 to 3.6 and a proper range of illumination intensity L = 2000–5000 cd/m^2. In the CTF measurements, the contrast of each available pattern is calculated using the following formula [24]:

$$C = \frac{I_{max} - I_{min}}{I_{max} + I_{min}} \tag{12}$$

Where C represents the pattern contrast of specific spatial frequency, I_{max} and $I_{\min}$ are the mean maximum and minimum gray values of the patterns. Based on the results calculated by Equation (12), the CTF for each s value can be constructed. In each CTF curve, the spatial cut-off frequency at which the contrast just reaches $C = 0$ can be used to describe the resolving power of the objectives [25, 26].

2.4. Condenser impact on DOF and the measuring method

The DOF defined as the axial range in the object space where the object is imaged with an acceptable deterioration is a key feature of the cytogenetic imaging and of the stability of the microscopic system especially when the system is used for continuous scanning [15, 27]. Generally, the total system DOF is regarded as the sum of geometric DOF and diffraction-limited DOF, of which the calculating formula for digital microscope system is shown below [15]:

$$DOF = \frac{ne}{\beta NA_{eff}} + \frac{nl}{NA_{eff}^2} \tag{13}$$

Where the first term is the geometric DOF and the second term is the diffraction-limited DOF; n is the refractive index of the medium between the objective front lens and the object; e is the smallest distance resolved by the high-resolution CCD; β is the magnification of the objective lens; λ is the wavelength of the light used in the microscope and NA_{eff} is the effective NA, which is NA_{obj} when $NA_{cond} \geq NA_{obj}$ and is $(NA_{obj} + NA_{cond})/2$ when $NA_{cond} \leq NA_{obj}$.

Based on the relationship between NA_{obj} and NA_{cond}, it is shown that the microscope's DOF can be enlarged by decreasing the NA_{cond} when $NA_{cond} \leq NA_{obj}$ and will keep as a constant value when $NA_{cond} \geq NA_{obj}$. The above assumptions will be verified by objective and subjective experiments using the 40× objective and under different s values. If the assumptions are valid, the restriction of DOF on system design and the implementation of algorithms such as autofocusing would be reduced greatly and system working stability would be significantly improved.

A specific range of spatial frequencies was chosen from the 1951 USAF resolution test chart to evaluate the condenser impact on DOF under the 40× objective. The resolution test chart was first located on the motorized stage and the well-focused position was visually determined by manually adjusting the height of the stage. Then, starting from the well-focused position, the stage first was moved up in succession with 20 steps (at interval 0.5 μm), and then moved down with

40 steps to avoid the backlash error caused by gear when changing the moving direction. At each step, the image of the resolution test chart was captured and its overall image sharpness was calculated using Equation (1). Finally, the focusing evaluation curves were plotted and the DOF values were determined and compared under the conditions of different *s* values.

2.5. Subjective evaluations of the condenser impact on cytogenetic imaging

Since the prototype microscopic imaging system used in this study was previously developed for cytogenetic imaging, large numbers of cytogenetic specimens (including bone marrow and blood), which were prepared by Health Sciences Center, University of Oklahoma (OUHSC), were used to subjectively assess the impacts of the condenser on image quality and DOF under the 40× objective. Chromosome bandings, which refer to the production of longitudinal differentiation along chromosomes by the use of special staining methods, were observed and their bands sharpness and contrast were compared under different conditions of *s* value [11].

Three steps were applied to conduct the subjective evaluations on the images obtained under the well-focused and the defocused conditions, separately. First, the whole image qualities of the determined region of interest (ROI) chosen from each sample under different *s* values were evaluated and their sharpness values were calculated by Equation (1). Then, typical chromosomes in each ROI were enlarged to describe the impact of the condenser on the details and their density profiles were established to record the average grayscale value of each perpendicular line across the approximated medial axis [3]. Finally, analyzable and non-analyzable chromosomes were divided based on the different density profile shape and the numbers of the analyzable chromosomes were counted and compared under different *s* values.

3. Results

3.1. The measurements of the condenser impact on image sharpness

For the measurements of the condenser impact on image sharpness, three different ranges of spatial frequencies (f) were selected from the 1951 USAF resolution test chart, and the corresponding image sharpness values were calculated using formula (1) under consecutive NA_{cond} (from 0.05 to 0.90 at interval 0.05) and proper ranges of illumination intensity. All the images were captured under the well-focused condition and the measuring results were shown in Figs. 4 and 5.

Based on the measuring results shown in Figs. 4 and 5, the best image sharpness can be obtained when *s* is in the range of 0.5–0.7 under any spatial frequencies and the proper illumination intensity (the high evaluation values are calculated when $L = 4000\ cd/m^2$ for the 10× objective and $L = 9000\ cd/m^2$ for the 40× objective).

3.2. The measurements of the condenser impact on resolution

The 1951 USAF resolution test chart and the 10× objective were applied to evaluate the condenser impact on resolution. The CTF was calculated under different *s* value from 0.2 to 3.6 and a proper range of illumination intensity $L = 2000–5000\ cd/m^2$. As an example, the CTF and its spatial cut-off frequency under the condition $L = 3000\ cd/m^2$ and $s = 0.2$ was shown in Fig. 6. Using the same method, all the spatial cut-off frequencies under $s = 0.2–3.6$ and $L = 2000–5000\ cd/m^2$ can be determined and their relations with *s* value are curved in Fig. 7.

According the measuring results in Fig. 7, the highest spatial cut-off frequency (i.e. the resolving power or the resolution) is obtained when *s* is set in the range of 0.6–0.8. All the above images are captured under the well-focused condition.

3.3. The measurements of the condenser impact on DOF

A specific range of spatial frequencies from 45.3 lp/mm to 57.0 lp/mm chosen from the 1951 USAF resolution test chart was selected to evaluate the condenser impact on DOF under the 40× objective. All the focusing evaluation curves under conditions of $s = 0.6$, 0.8, 1.0 and 1.2 are plotted in Fig. 8 using the method described in section 2.4. The consideration that the evaluation range of *s* is set in 0.6–1.2 based on the results from section 3.1 and 3.2. The image sharpness values reach their maximums at the

(a)

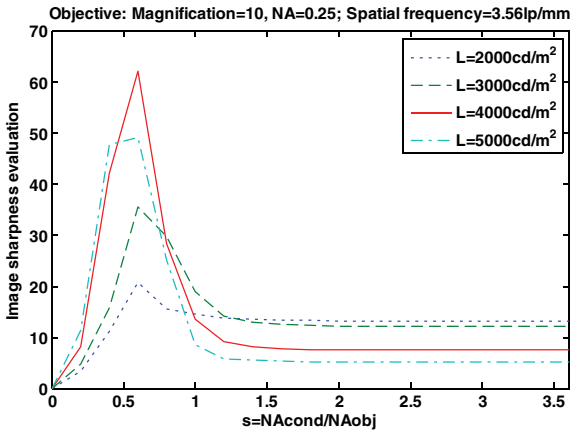

(b)

(c)

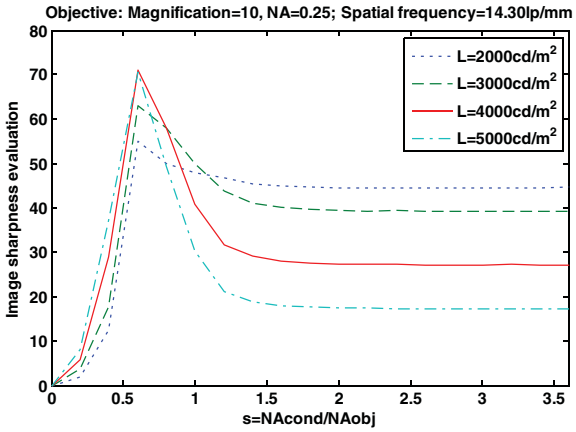

(d)

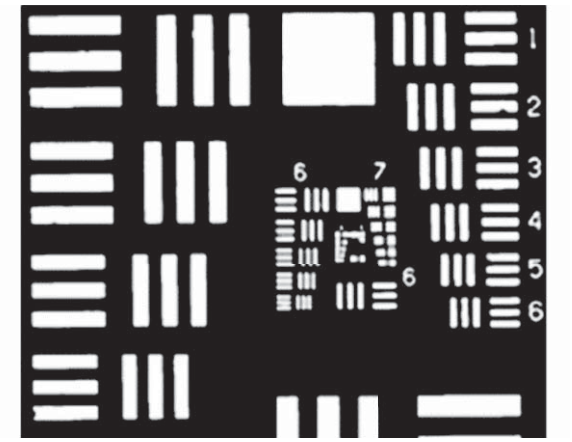

(e)

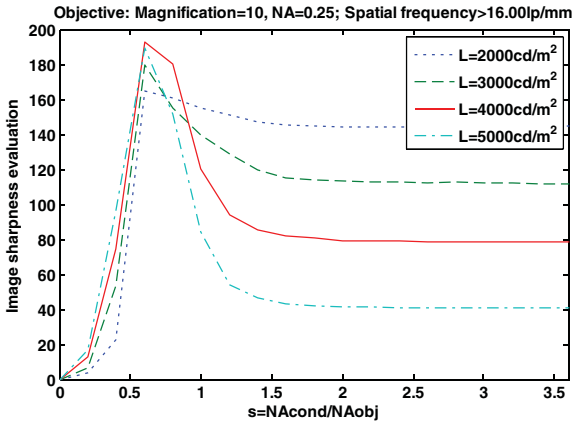

(f)

Fig. 4. The image sharpness measurements under 10× (dry, $NA_{obj} = 0.25$) with illumination intensity in the rangeof L = 2000–5000 cd/m^2; the L subjects to various systems; (a) f = 3.56 lp/mm; (b) the measuring results of (a); (c) f = 14.30 lp/mm; (d) the measuring results of (c); (e) f > 16.00 lp/mm; (f) the measuring results of (e).

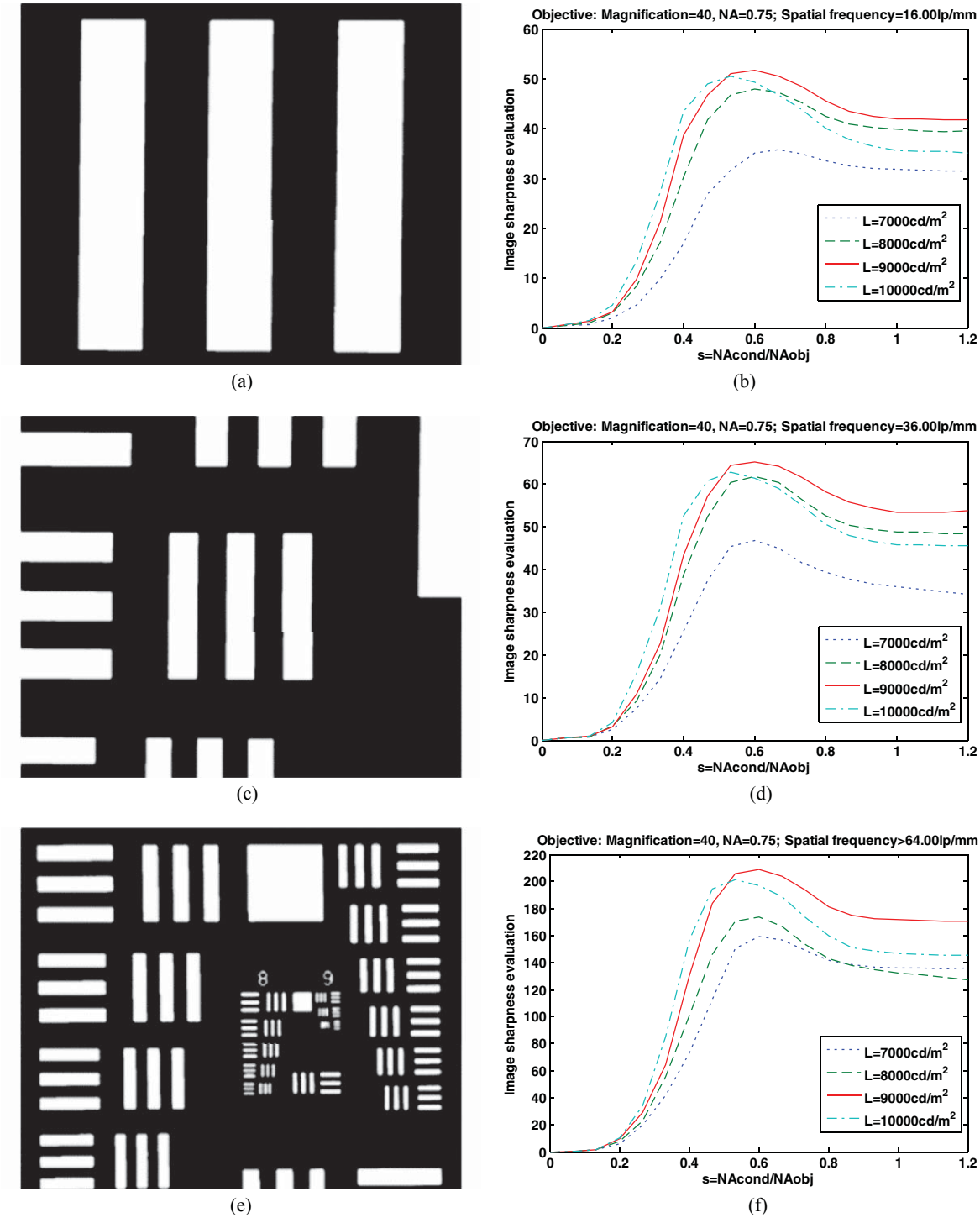

Fig. 5. The image sharpness measurements under 40× (dry, $NA_{obj} = 0.75$) with illumination intensity in the range of L = 7000–10000 cd/m^2; the L subjects to various systems; (a) f = 16.00 lp/mm; (b) the measuring results of (a); (c) f = 36.00 lp/mm; (d) the measuring results of (c); (e) f > 64.00 lp/mm; (f) the measuring results of (e).

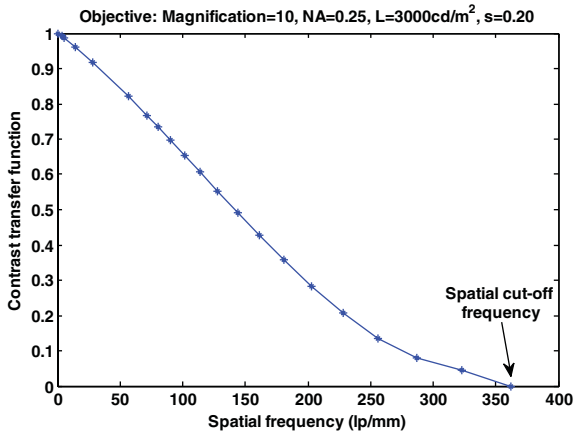

Fig. 6. The CTF curve and the corresponding spatial cut-off frequency under the condition: 10× (dry, $NA_{obj} = 0.25$), L = 3000 cd/m^2 and $s = 0.2$.

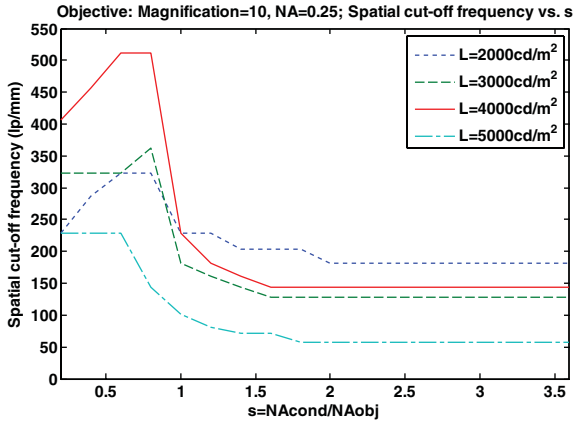

Fig. 7. The relation between spatial cut-off frequencies and s values under different light illumination conditions; the highest spatial cut-off frequency is obtained when $s = 0.6$–0.8 under L = 2000–4000 cd/m^2. For L = 5000 cd/m^2, the spatial cut-off frequency (resolution) is quite low due to too much flare (stray light), which lowers the pattern contrast.

well-focused position (z = 0 μm) under each condition of s, and decrease when being moved away from the focal plane. If the evaluation value 50.0 (the broken horizontal red line in Fig. 8) is used as the sharpness threshold, and the distance between the two thresholds is defined as DOF, it is shown that the largest DOF is obtained under $s = 0.6$, and the DOF decreases with the increase of s from 0.6 to 1.2. The changing tendency of the DOF values coincides with the theoretical analysis [3, 20].

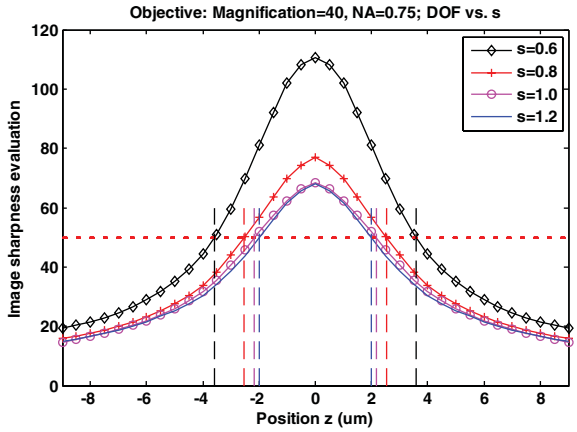

Fig. 8. The measured image sharpness versus focusing positions under the 40× objective and different s values: 0.6, 0.8, 1.0, and 1.2.

3.4. *The subjective evaluations of the condenser impact on cytogenetic imaging*

Ten samples including blood and bone marrow were chosen to conduct the subjective evaluation under the 40× objective and different s (0.6, 0.8, 1.0 and 1.2). As an example, the images acquired from a random ROI of one sample are shown in Fig. 9, in an effort to demonstrate the impact of the condenser.

First, Equation (1) is used to calculate the overall image sharpness values which are 64.8046, 60.7250, 55.6022 and 53.5208 for $s = 0.6$, 0.8, 1.0 and 1.2, respectively. The results show that the image sharpness decreases with the increase of s from 0.6 to 1.2. Then, two typical chromosomes in each ROI image are enlarged to describe the impact of the condenser on the details and then the density profiles are established to record the average gray value of each perpendicular line across the approximated medial axis. The corresponding density profiles of the right one of the two enlarged chromosomes are shown in Fig. 10 in which the local valley of the profile represents the dark band, while the local peak corresponds to the white band. The number of peaks and valleys in the density profile determines the number of black and white bands in the chromosome.

Although the overall image resolution is somewhat low due to the translucent sample, low magnification and NA_{obj} of the objective, the chromosome band patterns A, B, C and D under $s = 0.6$ and 0.8 (Figs. 9(a), (b) and 10(a), (b)) are much sharper and clearer. They are recognizable and adequate for clinical

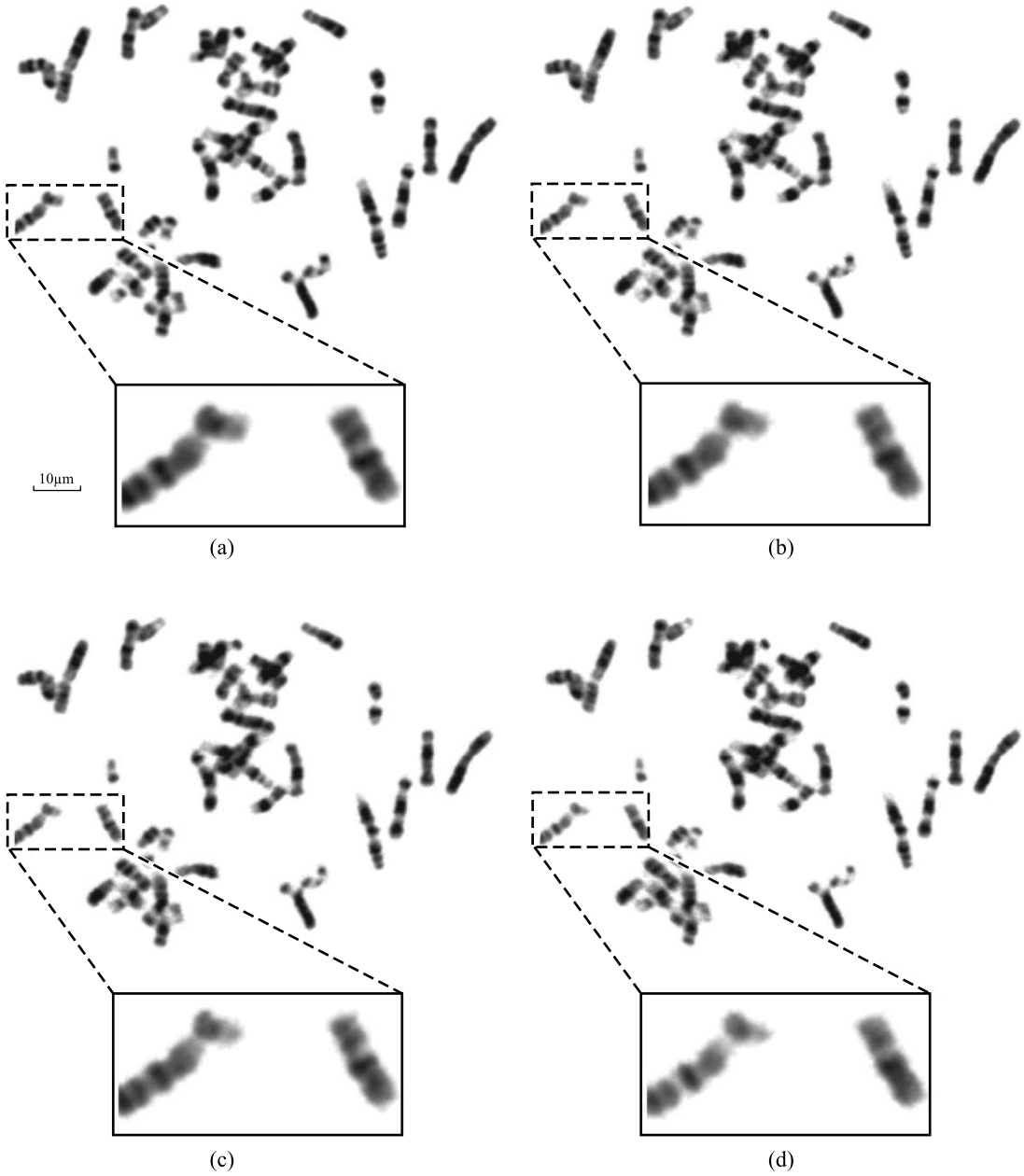

Fig. 9. Microscopic images acquired from the one sample under the 40× objective and different value *s*: (a) $s = 0.6$ (b) $s = 0.8$ (c) $s = 1.0$ (d) $s = 1.2$.

diagnosis. Figures 9(c) and 10(c) show a decreased image quality and band patterns sharpness, but it is still recognizable. However, the band patterns under $s = 1.2$ in Figs. 9(d) and 10(d) are barely recognizable in which bands A and B are difficult to be separated with each other even using post-processing method.

Based on the analysis of density profiles in Fig. 10, the chromosomes in (a), (b) and (c) can be regarded as analyzable chromosomes; otherwise it is non-analyzable as shown in (d). All the chromosomes in the ten ROIs from the ten samples, therefore, can be analyzed using the density profile based method. The numbers of analyzable chromosomes in each ROI

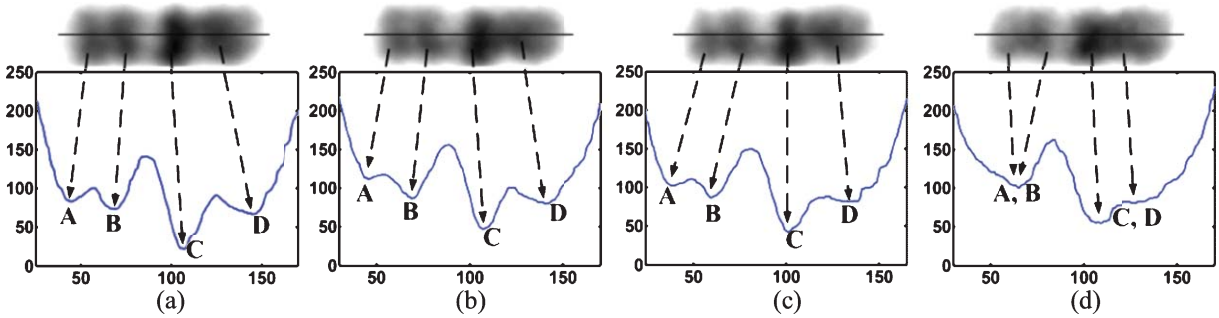

Fig. 10. The density profiles of a typical chromosome used to analyze the impact of the condenser on chromosome bands under 40× objective and different value s: (a) $s = 0.6$ (b) $s = 0.8$ (c) $s = 1.0$ (d) $s = 1.2$; it is shown that bands A and B can be separated in (a), (b) and (c), but can't in (d). Also, bands C and D in (d) have the decreased contrast compared with those in (a), (b) and (c).

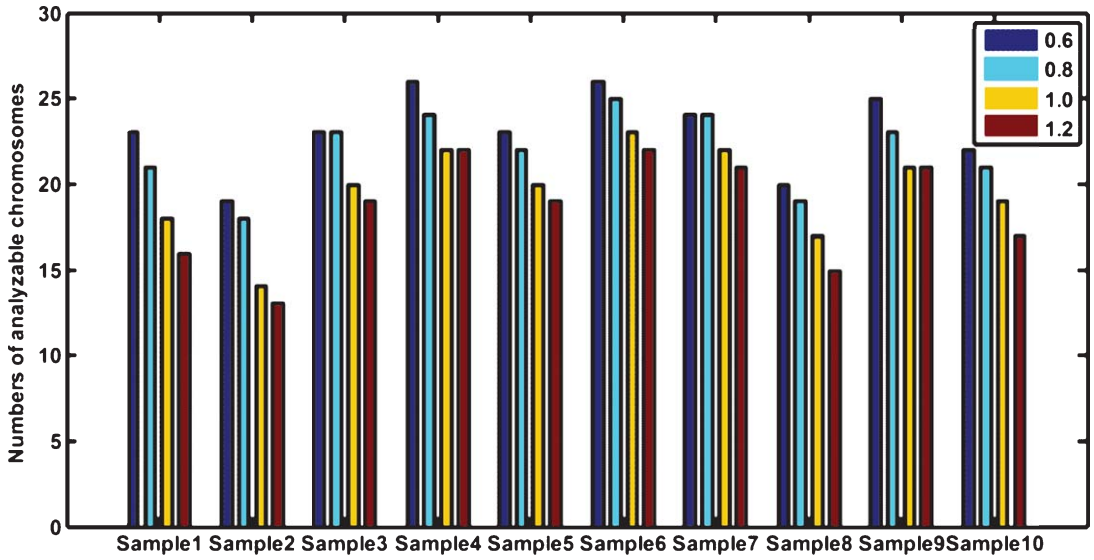

Fig. 11. The statistical result of the numbers of the analyzable chromosomes when all the samples are observed under the well-focused condition; for each sample, four bars from left to right represent the number of analyzable chromosomes under well-focused condition of $s = 0.6$, 0.8, 1.0 and 1.2, respectively.

under different s are shown in Fig. 11. The results show that there are more analyzable chromosomes under $s = 0.6$ and 0.8 than those under $s = 1.0$ and 1.2.

Based on the preceding experiments, all the samples are then observed 1 μm below the well-focused plane under $s = 0.6$, 0.8, 1.0 and 1.2, in an effort to subjectively evaluate the condenser influence on DOF and system working stability. The defocused images of the same ROIs (Fig. 9) are shown in Fig. 12 for comparison. The sharpness values also evaluated by Equation (1) are 43.1464, 40.3433, 37.2386 and 35.2497 for $s = 0.6$, 0.8, 1.0 and 1.2, respectively. In the same enlarged typical chromosomes, the left one that can be recognized when $s = 0.6$–1.2 under the well-focused condition, are still clear under the defocused condition with $s = 0.6$ and 0.8. However, the banding patterns become difficult to be distinguished under $s = 1.0$ and 1.2. Then, after applying the density profile based method, the numbers of the analyzable chromosomes in ten ROIs are also counted and shown in Fig. 13.

The results show that when the stage is moved away from the well-focused point at the same distance such as 1 μm, there are more analyzable chromosomes under $s = 0.6$ and 0.8. It means that under the same defocused condition, the system with $s = 0.6$ and 0.8 has higher stability than with $s = 1.0$ and 1.2. The results of observations are in agreement with those of using the resolution test chart.

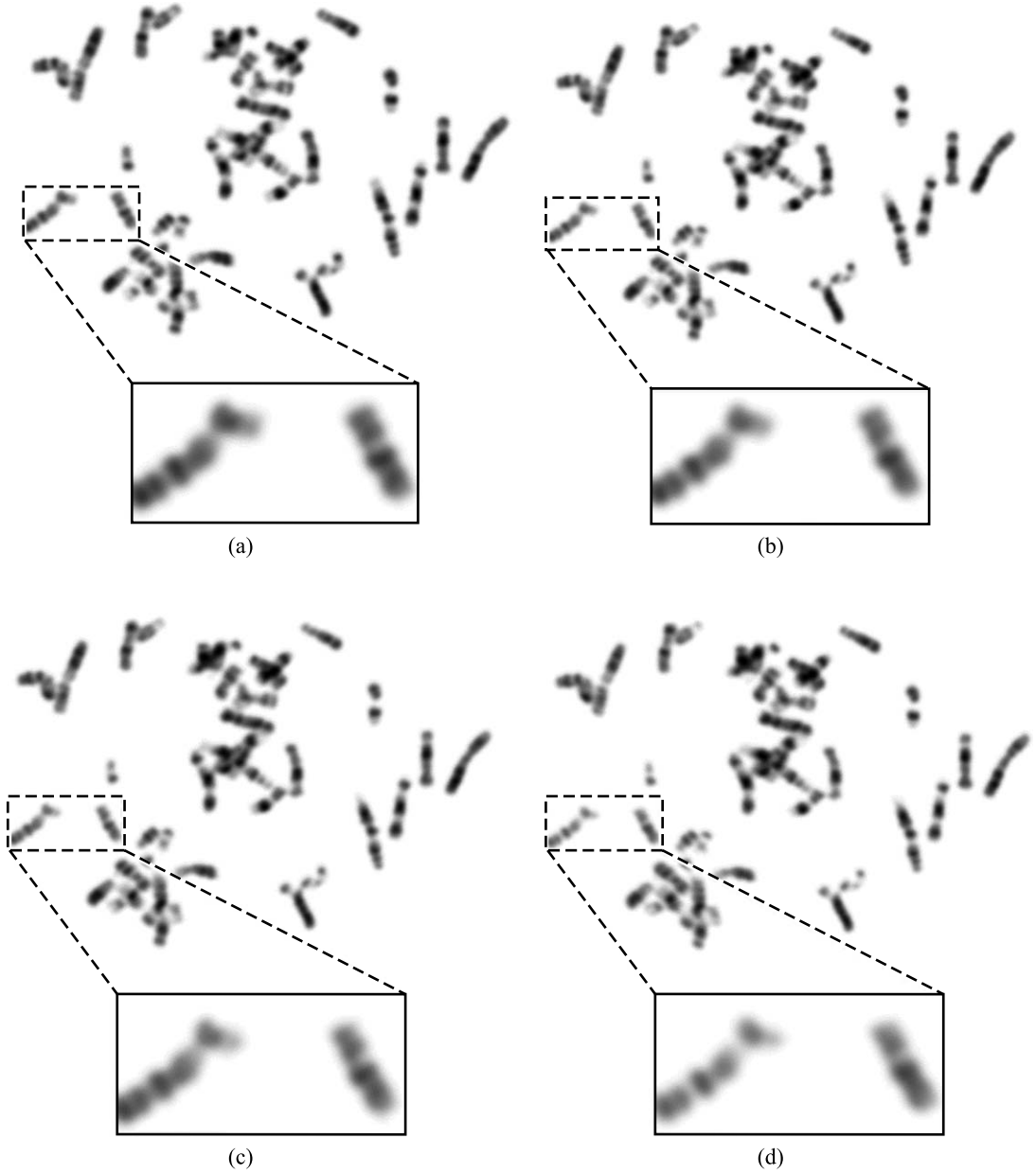

Fig. 12. Microscopic images from the same sample acquired under the 40× objective at the position 1 μm below the focal plane; the corresponding value s are: (a) $s = 0.6$ (b) $s = 0.8$ (c) $s = 1.0$ (d) $s = 1.2$.

4. Discussions and conclusions

The digital optical microscopic imaging systems are principal tools used in cytogenetic image analysis and diagnosis. As one of the most significant components in the optical microscopes, the condenser controls the illumination intensity and the angle of light entering the front lens of the objective, and then impacts the image sharpness, resolution, and DOF and the imaging quality of the whole system. Thus, understanding the condenser impacts and finding out the optimal relationship between the condenser and the objective based on the theoretical analysis and the comprehensively experimental validations is a critical issue for

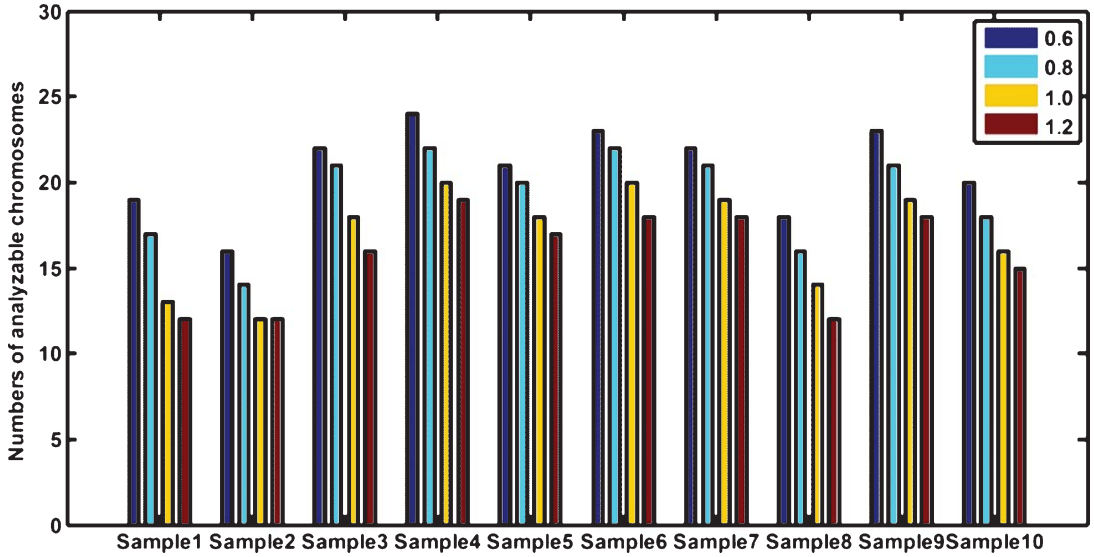

Fig. 13. The statistical result of the numbers of the analyzable chromosomes when all the samples are observed under the defocused (1 μm) condition; for each sample, four bars from left to right represent the number of analyzable chromosomes under defocused condition of $s = 0.6$, 0.8, 1.0 and 1.2, respectively.

optimizing operational parameters of digital optical microscopes.

Based on the objective experiments using the resolution test chart, it is concluded that the best image sharpness can be obtained when s is set in the range of 0.5–0.7 under proper illumination intensity ($L = 4000\,cd/m^2$ for the 10× objective and $L = 9000\,cd/m^2$ for the 40× objective) and any spatial frequencies; while to yield the optimal system resolution the s range should be set in 0.6–0.8. This experimental result regarding optimal resolution is a bit different from the conclusions derived based on Equations (2) and (3), or Equation (5), but agrees with the hypothesis that the optimal size or range of the condenser aperture should be a little smaller than that when $s = 1$. The reason is that when the aperture diaphragm of the condenser is opened greater than that of the objective, the flare (stray light) not only influences the image sharpness, but also lowers the pattern contrast, then reduces the system resolution. However, the flare (stray light) can be well reduced by setting s in the above range while sufficient illumination can be provided. In general, s can be set in the range of 0.6–0.7 to compromise optimal image sharpness and best spatial resolution in the specific prototype system reported in this study. The conclusion is also supported by the subjective observation and analysis of the images acquired from the cytogenetic specimens.

Also, the DOF can be effectively enlarged under the range of $s = 0.6$–0.7 when compared with larger condenser aperture ($s \geq 1$) or even its full open. Large DOF is quite important and meaningful for a digital microscope imaging system especially when it is used for high throughput continuous image scanning of cytogenetic specimens. The restrictions and requirements of autofocusing methods, for example, can be effectively reduced because the system with large DOF has much higher tolerance of variability coming from the specimen, which makes the system have higher stability and enhanced working performance. Also, much more clinical information such as analyzable chromosomes and their details can be observed and detected under such a condition resulting in the significant improvement of diagnostic efficiency and accuracy [28].

This study focused on investigating and testing the impact of the condenser combining with modern digital microscopic imaging system on the biomedical applications. More importantly, the study presented a much more comprehensive evaluation results and information to understand how to select the optimally operational parameters used in the microscopic condenser when integrating to the digital microscope imaging system. However, there are still some limitations in this study. For example, only 10× objective was used to evaluate the impact of the condenser on

resolution due to the spatial frequency limit (645.0 lp/mm) of the 1951 USAF resolution test chart and no objectives with much higher magnification such as 60× and above were applied because the maximum of the condenser aperture in this prototype system is 0.90. As a further step, therefore, much more comprehensive experiments should be conducted such as using another resolution test chart with higher spatial frequency to evaluate the condenser impact on resolution under the 40× objective. Also the oil immersion objectives combined with the supporting condenser, of which the NA_{cond} is up to 1.25 or higher, should be tested because much more information and details for clinical diagnosis can be provided due to their high magnification and resolving power.

In summary, we analyzed the chromosome banding details imaged using a microscopic image scanning system and illustrated the impact of the condenser on cytogenetic imaging quality and the system working stability intuitively. Moreover, the presented measuring methods and the optimal parameter of the condenser may offer useful guidelines for designing the optimally operational parameters in cytogenetic imaging using the high throughput continuous scanning microscopes in the future studies.

Acknowledgments

This research is supported in part by National Institutes of Health (NIH) grants RO1 CA 115320, RO1 CA136700 and supported in part by a grant from the University of Oklahoma Charles and Peggy Stephenson Cancer Center funded by the Oklahoma Tobacco Settlement Endowment Trust. The authors would like to acknowledge the support of Charles and Jean Smith Chair endowment fund as well.

References

[1] J.H. Tjioand and A. Levan, The chromosome number in man, *Hereditas* **42** (1956), 1–6.

[2] J.A. Book, A proposed standard system of nomenclature of human mitotic chromosomes, *Eugen Rev* **52** (1960), 1063–1065.

[3] X.W. Wang, B. Zheng, S.B. Li, J.J. Mulvihill and H. Liu, A rule-based computer scheme for centromere identification and polarity assignment of metaphase chromosomes, *Comput Meth Prog Bio* **89** (2008), 33–42.

[4] J. Piper, A review of high-grade imaging of diatoms and radiolarians in light microscopy optical- and software- based techniques, *Diatom Res* **26** (2011), 57–72.

[5] X.W. Wang, B. Zheng, S.B. Li, J.J. Mulvihill, X.D. Chen and H. Liu, Automated identification of abnormal metaphase chromosome cells for the detection of chronic myeloid leukemia using microscopic images, *J Biomed Opt* **15**(4) (2010), 046021:1–12.

[6] E. Grisan, E. Poletti and A. Ruggeri, Automatic segmentation and disentangling of chromosomes in Q-band prometaphaseiamges, *IEEE Trans Inf Technol Biomed* **13**(4) (2009), 575–581.

[7] X.W. Wang, B. Zheng, S.B. Li, J.J. Mulvihill, M.C. Wood and H. Liu, Automated classification of metaphase chromosomes: Optimization of an adaptive computerized scheme, *J Biomed Inf* **42** (2009), 22–31.

[8] M.W. Davidson and M. Abramowitz, Optical microscopy, in *Encyclopedia of Imaging Science and Technology*, Vol. II, J. Hormak, Ed., Wiley-Interscience, New York, 2002, pp. 1106–1141.

[9] H. Osterberg and L.W. Smith, Effects of numerical aperture on contrast in ordinary microscopy, *J Opt Soc Am* **51**(7) (1961), 709–714.

[10] S. Bell and K. Morris, *An introduction to microscopy*, CRC Press, New York, 2010.

[11] A.J. Lacey, *Light microscopy in biology: A practical approach*, 2nd edition, Oxford University Press, New York, 1999.

[12] J. Rittscher, R. Machiraju and T.C. Stephen Wong, *Microscopic image analysis for life science applications*, Artech House, Norwood, 2008.

[13] H.H. Hopkins and P.M. Barham, The influence of the condenser on microscopic resolution, *Proc Phys Soc B* **63**(737) (1950), 737–744.

[14] H.G. Kapitza, Microscopy: From the very beginning, Carl Zeiss Jena GmbH, 1997.

[15] S. Inoue and R. Oldenbourg, Microscopes, Chap. 17 in *Handbook of Optics*, 2nd edition, Vol. II, M. Bass, Ed., McGraw-Hill, New York, 1995.

[16] M. Abramowitz, *Microscope basics and beyond*, Olympus Corporation Publishing, 1987.

[17] M.S. Elliot, Conventional optical microscopy of colloidal suspensions, *Adv Colloid Interface Sci* **92** (2001), 133–194.

[18] D.Y. Yu and H.Y. Tan, *Engineering Optics*, 2nd edition, Mechanical Industry Press, Beijing, 2000.

[19] J. James and H.J. Tanke, *Biomedical light microscopy*, Kluwer academic publishers, Dordrecht, 1991.

[20] O. Kim, The condenser aperture diaphragm, MicrobeHunter Dec. 18th 2008.

[21] H. Zhu, *Basic digital image processing*, Science Press, Beijing, 2005.

[22] X.D. Chen, B. Zheng and H. Liu, Optical and digital microscopic imaging techniques and applications in pathology, *Anal Cell Pathol* **34**(1-2) (2011), 5–18.

[23] M. Born and E. Wolf, *Principles of optics: Electromagnetic theory of propagation, interference and diffraction of light*, 7th edition, Cambridge University Press, London, 1999.

[24] W.J. Smith, *Modern optical engineering*, 4th edition, McGraw-Hill, New York, 2008.

[25] A.J. den Dekker and A. van den Bos, Resolution: A survey, *J Opt Soc Am A* **14**(3) (1997), 547–557.

[26] J.T. Bushberg, J.A. Seibert, E.M. Leidholdt and J.M. Boone *The essential physics of medical imaging*, 2nd edition, Lippincott Williams and Wilkins, Philadelphia, 2002.
[27] X.D. Chen, L.Q. Ren, Y.C. Chen and H. Liu, New method for determining the depth of field of microscope systems, *Appl Optic* **50**(28) (2011), 5524–5533.
[28] Y.C. Qiu, X.D. Chen, Y.H. Li, S.B. Li, W.R. Chen and H. Liu, Impact of the optical depth of field on cytogenetic image quality, *J Biomed Opt* **17**(9) (2012), 096017:1–7.